

Wide-ridge metal-metal terahertz quantum cascade lasers with high-order lateral mode suppression

Jonathan A. Fan,^{a)} Mikhail A. Belkin, and Federico Capasso^{b)}
Harvard School of Engineering and Applied Sciences, Harvard University, Cambridge, Massachusetts 02138, USA

Suraj P. Khanna, Mohamed Lachab, A. Giles Davies, and Edmund H. Linfield
School of Electronic and Electrical Engineering, University of Leeds, Leeds LS2 9JT, United Kingdom

(Received 20 November 2007; accepted 24 December 2007; published online 23 January 2008)

Terahertz quantum cascade lasers with wide-ridge metal-metal waveguides are prone to lasing in high-order lateral modes, which reduce the maximum light output power from these devices. We have demonstrated, theoretically and experimentally, that the output power can be improved severalfold by introducing “side absorbers” into the waveguide structure, which enforce lasing in the TM_{00} mode with minor temperature performance deterioration. Lasers without side absorbers operate up to 168 K, a current record for devices processed using indium/gold wafer bonding. © 2008 American Institute of Physics. [DOI: 10.1063/1.2835202]

Terahertz quantum cascade lasers (QCLs) are an emerging compact source of narrowband terahertz radiation in the wavelength range of 60–350 μm (5–0.85 THz).¹ In order to achieve lasing, the laser mode requires strong confinement within the active region. This challenge is addressed by the use of surface plasmon waveguides, of which two types have been reported: the semi-insulating surface-plasmon (SI-SP) waveguide² utilizes a metal film on top of the QCL active region and provides mode confinement of $\sim 15\%–50\%$.³ The MM waveguide^{4,5} comprises metal films on both sides of the active region and provides mode confinement of nearly 100%.^{3–5}

The MM waveguide design, compared to the SI-SP waveguide design, empirically provides the best temperature performance for terahertz QCLs,^{5,6} but it suffers from poor radiation out-coupling efficiency and a highly divergent far-field profile because the mode is confined to subwavelength dimensions.³ While some applications, such as heterodyne detection, do not require high output power, other applications such as imaging^{7,8} require both a good far-field profile and high output power. These parameters can be improved by using wide-ridge ($>100\ \mu\text{m}$) waveguides; however, we will show that wide-ridge MM waveguides are prone to high-order lateral mode operation. This is undesirable because it yields a highly divergent, multiple-lobe far-field profile. In addition, as we will further analyze, the facet reflectivity for higher order lateral modes is significantly higher than that for the TM_{00} mode, yielding reduced radiation out-coupling efficiency.

A number of approaches addressing the problem of poor terahertz outcoupling in MM terahertz QCLs have been proposed, including the use of a silicon microlens at the waveguide facet⁹ and surface-emission schemes that utilize second-order diffraction gratings^{10,11} or two-dimensional photonic crystal structures.¹² However, the positioning of a microlens onto the waveguide facet is difficult,⁹ and edge-

emitting lasers are significantly easier to fabricate than surface-emitting lasers.

In this letter, we demonstrate lasing mode control in wide-ridge MM terahertz QCLs. We fabricate 150- μm -wide edge emitting MM terahertz QCLs operating at 3 THz with thin strips of highly doped GaAs exposed along the ridge waveguide edges [the “side absorbers,” Fig. 1(a)]. These devices operate in the TM_{00} mode and demonstrate a threefold increase in power output with little temperature degradation compared to devices without side absorbers. We note that this laser mode control technique may be used to improve the outcoupling efficiency and the far-field profile for edge-emitting devices equipped with microlenses, and can be implemented in surface-emitting MM terahertz QCLs with

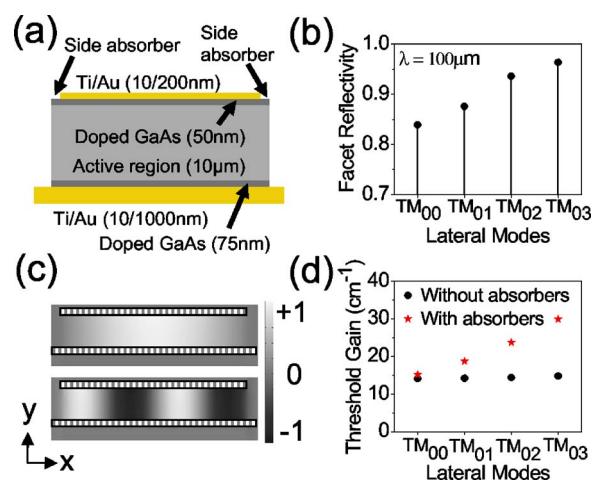


FIG. 1. (Color online) (a) Cross-sectional schematic diagram of the MM waveguide QCL with side absorbers. Layer thicknesses are marked in parentheses; the GaAs layers are doped to $5 \times 10^{18}\ \text{cm}^{-3}$. The side absorbers consist of exposed plasmon layer at the edges of the top metal cladding and are marked with arrows. (b) Facet reflectivity as a function of lateral mode order for a 10- μm -thick and 150- μm -wide MM waveguide. (c) Cross-section plots of the H_x component of two lateral waveguide modes. The upper plot is the TM_{00} mode and the lower plot is the TM_{03} mode. The metal waveguide claddings are shaded in vertical stripes. (d) Threshold gain as a function of lateral mode order for laser structures with and without side absorbers.

^{a)}Electronic mail: jfan@fas.harvard.edu.

^{b)}Electronic mail: capasso@seas.harvard.edu.

wide ridges, which suffer from high-order lateral mode lasing.^{10,11} We also report devices without side absorbers that operate up to a maximum temperature of 168 K, which constitutes the highest operating temperature achieved to date with MM terahertz QCLs processed using In/Au wafer bonding.

To understand the modal structure of the emission in wide-ridge MM devices, we calculated the lasing threshold for various lateral modes using COMSOL MULTIPHYSICS. First, we calculated the facet reflectivity for different lateral modes using three-dimensional simulations. We assumed a lossless active region with a refractive index of 3.5, a free space wavelength of 100 μm , and a perfectly conducting metal cladding. The waveguide width and thickness were chosen to be 150 and 10 μm , respectively. The simulation results are shown in Fig. 1(b); the facet reflectivity increases from 84% for the TM_{00} mode to 96% for the TM_{03} mode. The physical origin of the high facet reflectivity and subsequent low out-coupling efficiency for higher order lateral modes can be understood by considering the mode lobes as radiation sources at the laser facet: the lobes are separated by a distance much smaller than the free space wavelength due to the high mode confinement provided by MM waveguides [Fig. 1(c)]. This results in strong destructive interference for emission into free space.

To calculate the threshold gain g_{th} for the various waveguide modes, we used the expression $\Gamma g_{\text{th}} = \alpha_m + \alpha_{\text{wg}}$, where Γ is the mode confinement factor, α_{wg} is the waveguide loss, and α_m is the mirror loss calculated from the reflectivity data in Fig. 1(b). We first calculated α_{wg} by solving for modes in the 150- μm -wide waveguide structure depicted in Fig. 1(a) with and without 2.5- μm -wide side absorbers. We used the Drude model with relaxation constants $\tau=1$ ps and $\tau=0.1$ ps for lightly and heavily doped semiconductor layers, respectively.³ For the GaAs plasmon layers, n -doped at $5 \times 10^{18} \text{ cm}^{-3}$, we calculate the refractive index to be $5.93+23.32i$. The active region refractive index was calculated to be $3.49+0.0061i$ and the gold refractive index was taken from Ref. 13 to be $240+400i$. Waveguide losses from the 10-nm-thick top titanium cladding layer were neglected. The simulations indicate that for MM waveguides without side absorbers, α_{wg} and Γ are approximately the same for all lateral mode orders due to the very strong confinement provided by the MM waveguide. For example, the TM_{00} and TM_{01} modes have α_{wg} of 14.1 and 14.2 cm^{-1} , respectively, and Γ of 99% each. On the other hand, we obtained very different α_{wg} for different lateral modes in the MM waveguide with side absorbers. The threshold gain calculated for different lateral modes in a 1.3-mm-long MM waveguide with and without side absorbers is plotted in Fig. 1(d). For the waveguide without side absorbers, the TM_{00} , TM_{01} , and TM_{02} lateral modes all have thresholds of within 0.1 cm^{-1} of each other, indicating little mode discrimination between the TM_{00} and higher order lateral modes. For the waveguide with side absorbers, the TM_{00} mode clearly has the lowest threshold gain of all the lateral modes with mode discrimination on the order of a few cm^{-1} . Furthermore, the side absorbers introduce very small additional loss to the TM_{00} mode.

To demonstrate the improvement of power output from devices with side absorbers, we processed and characterized MM waveguide terahertz QCLs with and without side absorbers. The QCL material was grown by molecular beam

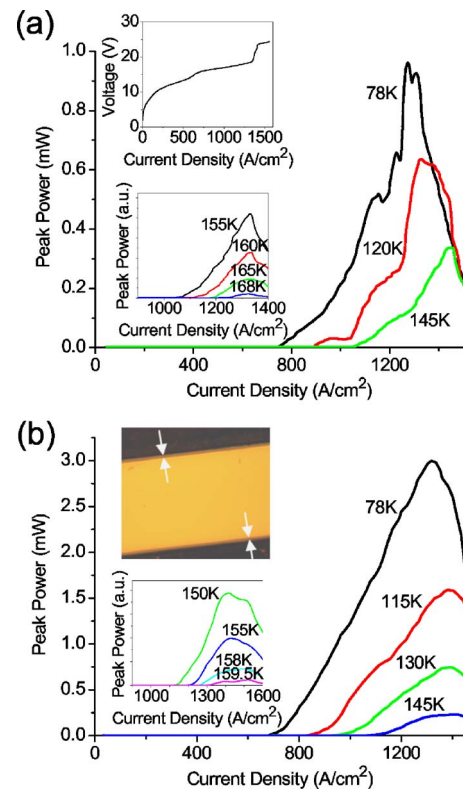


FIG. 2. (Color online) (a) Light output as a function of current (LI) of a representative MM waveguide device with no side absorbers. Upper inset: current-voltage characteristics of the device at 78 K. Lower inset: LI characteristics of the device close to the maximum operating temperature. (b) LI characteristics of a representative MM waveguide device with side absorbers. Upper inset: image of the top of a MM waveguide device with side absorbers delineated by arrows. Lower inset: LI characteristics of the device close to the maximum operating temperature.

epitaxy; the growth started with a 250-nm-thick GaAs buffer layer, followed by a 300-nm-thick $\text{Al}_{0.5}\text{Ga}_{0.5}\text{As}$ layer, a 75-nm-thick layer of GaAs n -doped to $5 \times 10^{18} \text{ cm}^{-3}$, $226 \frac{1}{2}$ stages of the active region design similar to that of Ref. 14 with a lower doping sheet density of $n_s=2.75 \times 10^{10} \text{ cm}^{-2}$, and finally a 50-nm-thick GaAs layer n -doped to $5 \times 10^{18} \text{ cm}^{-3}$. The material was processed into gold MM waveguides following the procedure outlined in Refs. 4 and 5. The 150- μm -wide ridges were defined via dry etching with a Microposit SU-8 2005 photoresist mask. After SU-8 removal, metal (Ti/Au, 10/200 nm) was evaporated on top of the laser ridges. Side absorbers were fabricated on some devices by depositing photoresist onto the ridges, opening thin strips along the ridge edges with optical lithography, and removing the strips of gold and titanium by wet etching. The final side absorbers were measured to be approximately 3- μm -wide [inset of Fig. 2(b)]. The processed wafers were cleaved into approximately 1.3-mm-long bars and indium mounted on gold-plated copper blocks.

The devices were placed in a helium flow cryostat and terahertz radiation was detected with a calibrated helium-cooled silicon bolometer. Light was collected with two 2 in. parabolic mirrors: one with a 5 cm focal length to collimate the light from the source, and another, 5 cm away from the first one, with a 15 cm focal length to refocus the light into the bolometer. The devices were operated in pulsed mode with 30 ns pulses at a 100 kHz repetition rate, with an additional 600 Hz modulation for lock-in detection. The light

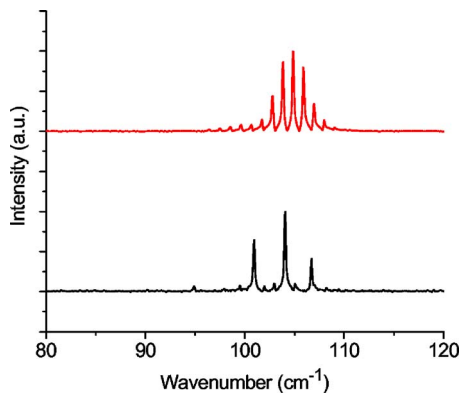


FIG. 3. (Color online) Representative spectra of lasers with (top) and without (bottom) side absorbers operating at a temperature of 78 K and a current density of 900 A/cm².

intensity-current (*LI*) and current-voltage (*IV*) characteristics of a representative device without side absorbers are shown in Fig. 2(a) for different heatsink temperatures. At a heatsink temperature of 78 K, the threshold current density was measured to be 710 A/cm² and the maximum peak power was measured to be 0.92 mW. The *LI* characteristics of a representative device with side absorbers are shown in Fig. 2(b). The threshold current density for this device at the heatsink temperature of 78 K was 685 A/cm², similar to that for devices without side absorbers, and the maximum peak power was measured to be 3.0 mW, which is over three times larger compared to that from devices without side absorbers.

Representative emission spectra of the devices with and without side absorbers are shown in Fig. 3. The mode spacing in the spectra of the device without side absorbers is nonperiodic, indicating lasing in multiple lateral order modes. In comparison, devices with side absorbers showed emission spectra with mode spacing indicative of Fabry Perot lasing under a single lateral mode. The spectra and enhanced power outcoupling indicate that the side absorbers enforce lasing in the TM₀₀ mode.

The devices without side absorbers operated up to a maximum temperature of 168 K [see Fig. 2(a)], which is the highest reported temperature for terahertz QCLs processed with In/Au bonding. We note that the gold MM waveguide devices reported in the original publication¹⁴ operated only up to 142 K. The improved performance of our devices may stem from better growth and/or processing quality, as well as lower doping density. The devices with side absorbers had a slightly worse temperature performance, with a maximum

operating temperature of ≈ 160 K [see Fig. 2(b)]. This reduction in temperature performance is attributed to the small amount of losses introduced by the side absorbers. The exceptional temperature performance of our devices demonstrates the potential of a three-well design¹⁴ for increasing the maximum operating temperature of terahertz QCLs. We note that the temperature performance of our devices may be further boosted¹⁵ by using a copper cladding since copper has better thermal¹⁶ and optical¹³ properties than gold.

J.F., M.B., and F.C. acknowledge support from the AFOSR under Contract No. FA9550-05-1-0435 (Gernot Pomrenke). The structures were processed in the Center for Nanoscale Science (CNS) in Harvard University. Harvard-CNS is a member of the National Nanotechnology Infrastructure Network. J.F. acknowledges support from the NSF Graduate Fellowship. S.K., M.L., G.D., and E.L. acknowledge support from EPSRC (UK) and Her Majesty's Government Communications Centre.

¹B. S. Williams, Nat. Photonics **1**, 517 (2007).

²R. Köhler, A. Tredicucci, F. Beltram, H. E. Beere, E. H. Linfield, A. G. Davies, D. A. Ritchie, R. C. Iotti, and F. Rossi, Nature (London) **417**, 156 (2002).

³S. Kohen, B. S. Williams, and Q. Hu, J. Appl. Phys. **97**, 053106 (2005).

⁴K. Unterrainer, R. Colombelli, C. Gmachl, F. Capasso, H. Y. Hwang, D. L. Sivco, and A. Y. Cho, Appl. Phys. Lett. **80**, 3060 (2002).

⁵B. S. Williams, S. Kumar, H. Callebaut, Q. Hu, and J. Reno, Appl. Phys. Lett. **83**, 2124 (2003).

⁶G. Scalari, N. Hoyler, M. Giovannini, and J. Faist, Appl. Phys. Lett. **86**, 181101 (2005).

⁷A. W. M. Lee, Q. Qin, S. Kumar, B. Williams, and Q. Hu, Appl. Phys. Lett. **89**, 141125 (2006).

⁸J. Darmo, V. Tamosiunas, G. Fasching, J. Kroll, K. Unterrainer, M. Beck, M. Giovannini, J. Faist, C. Kremser, and P. Debbage, Opt. Express **12**, 1879 (2004).

⁹A. W. M. Lee, Q. Qin, S. Kumar, B. S. Williams, Q. Hu, and J. Reno, Opt. Lett. **32**, 2840 (2007).

¹⁰J. A. Fan, M. A. Belkin, F. Capasso, S. Khanna, M. Lachab, A. G. Davies, and E. H. Linfield, Opt. Express **14**, 11672 (2006).

¹¹S. Kumar, B. S. Williams, Q. Qin, A. W. M. Lee, Q. Hu, and J. Reno, Opt. Express **15**, 113 (2007).

¹²G. Scalari, L. Sirigu, R. Terazzi, C. Walther, M. I. Amanti, M. Giovannini, N. Hoyler, J. Faist, M. L. Sadowski, H. Beere, D. Ritchie, L. A. Dunbar, and R. Houdre, J. Appl. Phys. **101**, 081726 (2007).

¹³M. A. Ordal, L. L. Long, R. J. Bell, S. E. Bell, R. R. Bell, R. W. Alexander, Jr., and C. A. Ward, Appl. Opt. **22**, 1099 (1983).

¹⁴H. Luo, S. R. Laframboise, Z. R. Wasilewski, G. C. Aers, H. C. Liu, and J. C. Cao, Appl. Phys. Lett. **90**, 041112 (2007).

¹⁵M. A. Belkin, J. A. Fan, F. Capasso, S. Khanna, M. Lachab, A. G. Davies, and E. H. Linfield, Opt. Express (to be published).

¹⁶B. S. Williams, S. Kumar, Q. Hu, and J. Reno, Opt. Express **13**, 3331 (2005).